Raman, Infrared, and Theoretical Studies of Fluorofullerene $C_{60}F_{20}$

Alexey A. Popov,*,† Alexey A. Goryunkov,† Ilya V. Goldt,† Ivan E. Kareev,† Igor V. Kuvychko,§ Wolf-Dietrich Hunnius,‡ Konrad Seppelt,‡ Steven H. Strauss,§ and Olga V. Boltalina*,†,§

Department of Chemistry, Moscow State University, Moscow 119992, Russia; Institute of Inorganic Chemistry, Freie University Berlin, Germany; and Department of Chemistry, Colorado State University, Fort Collins, Colorado 80523

Received: August 22, 2004; In Final Form: October 5, 2004

Improved synthetic and isolation procedures have been developed that resulted in the preparation of pure $C_{60}F_{20}$ in sufficient amounts for comprehensive vibrational spectroscopic studies. The FTIR spectrum, the first Raman spectrum, and DFT vibrational calculations of the two possible D_{5d}-symmetry isomers of $C_{60}F_{20}$ provide compelling evidence in favor of the previously proposed Saturn-like structure of this fluorofullerene. Excellent agreement between the experimental and simulated spectra allowed a complete vibrational assignment for $C_{60}F_{20}$ to be made.

Introduction

Among the dozens of fluorine-containing fullerene derivatives that we have previously isolated from the products of high-temperature metal−fluoride reactions of [60]fullerene, $C_{60}F_{20}$ remains one of the most intriguing fullerene compounds described to date and yet the least studied. $C_{60}F_{20}$ was first isolated from the crude product of reaction between C_{60} and KF/MnF_3 mechanical mixture, showing a single line in the ^{19}F NMR spectrum, which indicated high symmetry of the molecule; only two of such D_{5d} isomers for $C_{60}X_{20}$ are theoretically possible.[1] The proposed structure **I** of $C_{60}F_{20}$ (Figure 1) with the belt of F atoms along the C_{60}-cage equator (reminiscent of planet Saturn) was favored mechanistically (the contiguous fluorine addition pattern is a characteristic feature for previously reported fluorofullerenes) and on the basis of the semiempirical calculations. The alternative D_{5d} structure (isomer **II** in Figure 1), which also satisfies the observed single-line ^{19}F NMR spectrum, was ruled out since it does not obey the mechanistic argument (i.e., it has the pattern with noncontiguous fluorines), and it was also found less stable (semiempirical calculations). No further structural elucidation has since been done due to unavailability of this compound.

Recently, Sandall and Fowler[2] showed that $C_{60}F_8$, which is formed under similar high-temperature conditions as $C_{60}F_{20}$,[3] does not possess the structure with contiguously added fluorine atoms, as originally conjectured. This example, along with the others,[4] shows that mechanistic approach cannot serve as a defining argument in the structural elucidation when NMR data do not provide a single solution.

In this work, we report the first vibrational spectroscopic studies of $C_{60}F_{20}$. Because of the recent progress in the synthesis and purification of the fluorofullerenes with low fluorine content,[5] which is partially described here, we were able to prepare sufficient quantities of the sufficiently pure $C_{60}F_{20}$ for the refined spectroscopic experiments. As an outcome of this work, which includes also the first-principle calculations of the geometry parameters, relative energies, and vibrational spectra of the possible isomers, we present a complete vibrational assignment for this fluorofullerene molecule.

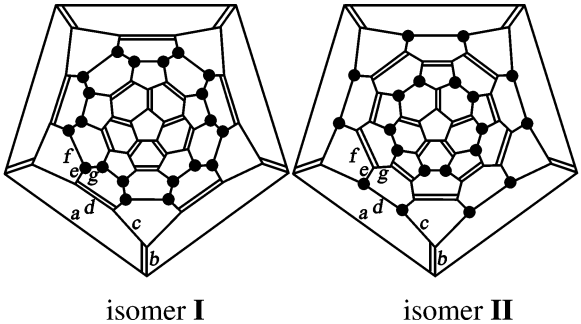

isomer **I** isomer **II**

Figure 1. Schlegel diagrams for D_{5d} $C_{60}F_{20}$ structures: "saturnene" (isomer **I**) and alternative structure (isomer **II**).

Experimental Section

Materials. C_{60} (Term USA, 99.9%), MnF_3 (Aldrich Chem. Co.), and KF (Aldrich Chem. Co., 99.99%) were used as received, and Li_4CeF_8 was prepared by treatment with F_2 (350 °C, 6 h) of the mixture of alkali metal chloride and CeO_2 taken in the respective stoichiometric amounts; a good correspondence with the reported XRD data was observed,[6] with some presence of the LiF phase.

Preparation and Isolation of $C_{60}F_{20}$. Details of the solid-state C_{60} fluorination procedures can be found elsewhere.[7] Briefly, volatile fluorination products, which are condensed in the cold part of the reactor, are collected and analyzed by the electron ionization (EI) and MALDI mass spectrometry, FT IR spectroscopy, and HPLC. Several reactions between C_{60} and Li_4CeF_8 were carried out at 390−460 °C, with molar ratio Li_4CeF_8/C_{60} ranging from 45 to 14, the typical overall yields were 30−50%, the highest yields of $C_{60}F_{20}$ were obtained for $Li_4CeF_8/C_{60} = 20$, these crude products were used for further processing. Reaction of C_{60} with $KF-MnF_3$ was performed

† Moscow State University.
‡ Freie University.
§ Colorado State University.
* To whom correspondence should be addressed. E-mail: A.A.P., popov@phys.chem.msu.ru; O.V.B., ovbolt@lamar.colostate.edu.

10.1021/jp046214a CCC: $27.50
Published on Web 12/01/2004

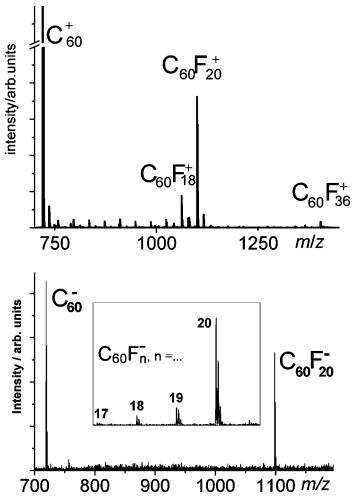

Figure 2. Top: positive ion EI (20 eV) mass spectrum of the crude product of reaction between C_{60} and KF/MnF_3. Bottom: negative-ion MALDI mass spectrum (S_8 matrix) of the purified $C_{60}F_{20}$. Inset: MALDI mass spectrum at the increased laser fluence.

under varying conditions: temperatures (430 and 480 °C), ratios of KF/MnF_3 (0.8−3.4-fold molar excess of KF), and MnF_3/C_{60} (17.7−22.3-fold molar excess of MnF_3). Two methods of preparation of $KF-MnF_3$ mixtures were applied: (i) vigorous grinding in inert atmosphere or (ii) in order to achieve better homogeneity annealing of the ground mixture in vacuo at elevated temperatures (330−520 °C) for 20 h. In the reaction of C_{60} with the mechanical mixture KF/MnF_3 (3.4/1.0 molar ratio) prepared by the former method, fluorination did not take place at all. Use of KF/MnF_3 (1.0−1.8/1.0 molar ratio) yielded mainly $C_{60}F_{36}$, with only small amounts of $C_{60}F_{18}$ and $C_{60}F_{20}$ (<3% according to the mass spectral and HPLC data). A series of the experiments with the annealed mixtures KF/MnF_3 resulted in the noticeable increase in the yields of lower fluorinated fullerenes. It was found, for example, that KF/MnF_3 (1/1 molar ratio, annealed at 430−450 °C) reacted with C_{60}, affording higher yields of $C_{60}F_{18}$ and $C_{60}F_{20}$ as compared to $C_{60}F_{36}$. Attempts to apply either higher KF/MnF_3 ratios and/or higher annealing temperatures did not give better results, leaving most of C_{60} unreacted. Use of the lower molar ratio of KF/MnF_3 mixture and/or lower annealing temperatures resulted in the increase in the $C_{60}F_{36}$ yield, as expected.

For the isolation of pure $C_{60}F_{20}$ samples, a two-stage chromatographic procedure was developed. Crude $C_{60}F_x$ samples were dissolved in toluene and filtered using a 0.45 μm filter in order to remove insoluble impurities (mainly of inorganic origin). At the first separation stage, Cosmosil Buckyprep (20 mm i.d. × 250 mm, Nacalai Tesque Inc.) with a high injection volume (18 mL injections, 18 mL/min flow rate, toluene eluent) was used, affording initial isolation of the $C_{60}F_{20}$ fraction eluting at 84 min (8.8 min, C_{60}). At the second stage, Regis Buckyclutcher (20 mm i.d. × 250 mm, Regis Chemical Co.) (1.2 mL injections, 12 mL/min flow rate, toluene eluent) was applied for the final purification from the compounds coeluting with $C_{60}F_{20}$ in the Cosmosil column. $C_{60}F_{20}$ (retention time 9 min, MALDI mass spectrum is shown in Figure 2) was thus separated from other components, which were identified by the MALDI method: $C_{60}F_{20}O$ (9.8 min), $C_{60}F_{14}$ (11.5 min), $C_{60}F_{12}$ (14 min). The latter two components were isolated for the first time, and their spectroscopic characterization will be reported in due course. The ^{19}F NMR spectrum of isolated $C_{60}F_{20}$: −134.5 ppm (376 MHz, Bruker, C_6D_6, C_6F_6 as a standard).

Instrumentation. Mass spectrometric analysis of the crude products from all reactions was carried out using the Quattro MS (Fisons) instrument supplied with an EI source, operating at 20 eV ionizing energy in order to suppress significant fragmentation. Mass spectrometric analysis of the HPLC-purified samples was performed with a matrix-assisted laser desorption/ionization time-of-flight (MALDI TOF) technique using a Voyager-DE PRO Biospectrometry workstation (Applied Biosystems). Radiation pulses of 0.5 ns and frequency 3 Hz from N_2 laser operating at 337 nm were used to desorb the species into the gas phase, and the negative ions formed were detected in the reflectron mode. Sulfur was used as a matrix: its solution in toluene was mixed with the $C_{60}F_{20}$ toluene solution prior to deposition onto the target. Raman spectra were recorded on the FT-Raman spectrometer RFS 100 (Bruker), with the resolution 3 cm^{-1}, 1000 scans, in the range 100−2000 cm^{-1}. The FT-IR spectrum (KBr pellet) was recorded with the use of Nicolet Avatar 320FT-IR, with the resolution 2 cm^{-1}.

Theoretical Methods. Molecular structures, harmonic vibrational frequencies, and IR transition probabilities were calculated at the DFT level of theory with the PRIRODA package[8] using GGA functional of Perdew, Burke, and Ernzerhof (PBE).[9] TZ2P-quality Gaussian basis set {6,1,1,1,1,1/4,1,1/1,1} was used for carbon and fluorine atoms throughout the calculations. The quantum-chemical code employed expansion of the electron density in an auxiliary basis set to accelerate the evaluation of the Coulomb and exchange-correlation terms. Raman intensities were computed numerically at the PBE/6-31G* level employing the PC version[10] of GAMESS (US) quantum chemical package.[11] Potential energy distribution analysis of the vibrational forms and scaling of the DFT force field were performed with the DISP[12] suite of programs for vibrational calculations. Cartesian DFT force field of $C_{60}F_{20}$ was transferred into redundant internal coordinate system, which included all chemical bonds and bond angles (totally 350 coordinates). Then internal force constants F_{ij}^{DFT} were scaled through the following equation:

$$F_{ij}^{scaled} = t_i^{1/2} F_{ij}^{DFT} t_j^{1/2}$$

where $t_{i,j}$ are scaling factors for internal coordinates i and j.

Results and Discussion

Preparation and Isolation of $C_{60}F_{20}$. Two significant improvements in the routine procedures, used for synthesis and isolation of fluorofullerenes, were first introduced in this work, which are responsible for the successful preparation of pure samples of $C_{60}F_{20}$.

First, we developed the synthetic approach allowing us to fine-tune fluorinating strength of the known fluorinating reagents, which resulted in the higher yields of fluorofullerenes with low fluorine content, and in particular $C_{60}F_{20}$. Two binary metal fluorides, MnF_3 and CeF_4, are known as good reagents for selective preparation of $C_{60}F_{36}$; particularly good results were obtained with the latter.[13] In this work, we applied two types of fluorinating agents based on the above binary fluorides: ternary rare earth metal fluoride, Li_4CeF_8, and mechanical mixtures $KF-MnF_3$.

An idea to use ternary metal fluorides instead of the high-valence binary metal fluorides is based on the following observations: (i) fluorofullerenes with low F content (n(F) ≤ 18−20) form more abundantly at higher temperatures (>420

TABLE 1: Optimized Geometry Parameters (Å) in D_{5d} $C_{60}F_{20}$

isomer	a	b	c	d	e	f	g	C−F
I	1.433	1.399	1.427	1.378	1.507	1.670	1.570	1.387
II	1.463	1.349	1.516	1.600	1.526	1.389	1.412	1.402

°C) than highly fluorinated homologues (RT−350 °C); (ii) complex metal fluorides (which are generally more stable with respect to reduction to lower valence state than corresponding binary fluorides) tend to react with fullerene at higher temperatures than binary metal fluorides (>450 °C).

Previously, we successfully used ternary fluoride K_2PtF_6 for preparation of $C_{60}F_{18}$.[5] However, this reagent does not afford sufficient quantities of other lower fluorinated fullerenes; particularly, $C_{60}F_{20}$ is formed only in negligible amounts (if at all). Therefore, a new reagent, Li_4CeF_8, was probed in this work. As mentioned above, reaction of C_{60} with binary Ce(IV) fluoride is known to yield selectively $C_{60}F_{36}$.[13] In contrast, reaction of C_{60} with Li_4CeF_8, as shown by mass spectral and HPLC analyses of the crude products, has resulted in the highest observed yields of the species with low n(F), $C_{60}F_{2,4,6,8}$ and, most importantly, drastic improvement in the $C_{60}F_{20}$ yields. Thus, the described synthetic approach based on the use of ternary metal fluorides as fluorinating agents is shown here as promising way for preparation of the fluorofullerenes with only a few attached F atoms, which are currently not available in sufficient macroscopic quantities.

The KF/MnF_3 system was used in our original paper,[1] and later, in the in situ Knudsen cell mass spectrometry (KCMS) work,[5] both studies showed formation of $C_{60}F_{20}$. Here, we have performed a systematic study of this system to optimize experimental parameters and achieve maximal yields of $C_{60}F_{20}$. The following variables were examined: (i) reaction temperature, (ii) ratio of KF and MnF_3, (iii) ratio between C_{60} and the fluorinating agent, and (iv) methods of preparation of the reaction mixture. As expected, by introducing KF in the reaction mixture, we achieved lower fluorinating activity as compared to pristine MnF_3; i.e., an increase in the relative abundance of fluorofullerenes $C_{60}F_n$ with $n < 36$ was observed. Furthermore, in some products, $C_{60}F_{20}$ was even more abundant than $C_{60}F_{18}$ (see Figure 2). However, the observed significant decrease in overall yields of fluorinated products made this reaction unsuitable for macroscopic preparations.

DFT-Optimized Geometry Parameters. A single-line ^{19}F NMR spectrum of the isolated $C_{60}F_{20}$ suggests D_{5d} symmetry, and only two such isomers are possible (Figure 1); the DFT-optimized geometry parameters for each structure are given in Table 1. Both structures are highly strained, and, therefore, it is instructive to compare angles and bonds adjacent to the fluorine-bearing carbon atoms in $C_{60}F_{20}$ with the corresponding parameters in the vicinity of the tertiary carbon atoms of the strain-free perfluoroadamantane molecule. In good agreement with the gas-phase electron diffraction values of 110.3(4)°, 1.560(3) Å, and 1.363(10) Å,[14] the PBE/TZ2P calculations yielded 109.4°, 1.568 Å, and 1.369 Å for CC(F)C angles, C(F)−C, and C(F)−F bonds in perfluoroadamantane molecule, respectively. Predicted C−F bond lengths in D_{5d} $C_{60}F_{20}$ isomers are 0.018 Å (**I**) and 0.033 Å (**II**) longer than the C(F)−F bond in perfluoroadamantane. In $C_{60}F_{20}$-**I**, the CC(F)C bond angles deviate considerably from the nearly tetrahedral values of $C_{10}F_{16}$ and constitute 102.7°, 111.0°, and 118.7° (for ∠**ef**, ∠**eg**, and ∠**fg**, respectively). Type **f** of the C(F)−C(F) bonds is substantially elongated (up to 1.670 Å), the feature resembling fluorofullerenes $C_{60}F_{18}$,[15] $C_{60}F_{36}$,[16] and $C_{60}F_{48}$ [17] with contiguous fluorine arrangement. Noteworthy, the longest C−C bond in

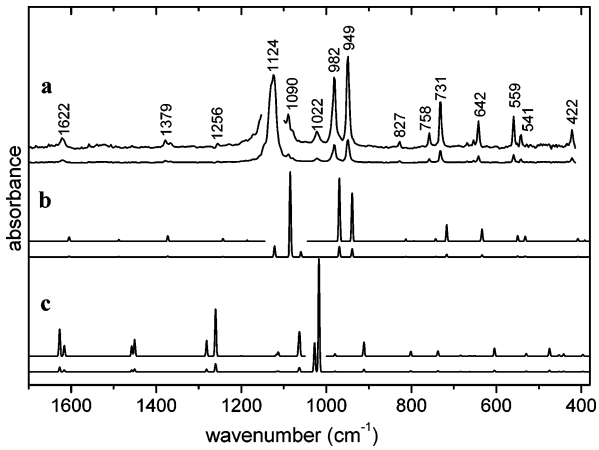

Figure 3. IR spectra of $C_{60}F_{20}$: (a) experimental (KBr pellet); (b) simulated for isomer **I** (saturnene); (c) simulated for isomer **II**.

structure **I** corresponds to the purely eclipsed conformation of FCCF moiety (i.e., corresponding dihedral FCCF angle being zero), whereas inherent strain for another FCCF fragment with the shorter C−C distance (**g**) is relaxed by the relative twisting of the eclipsed C−F bonds by 23° around C−C bond. In $C_{60}F_{20}$-**II**, the addition pattern comprises a noncontiguous series of 1,2 additions across 10 hexagon−hexagon edges. C(F)−C(F) bonds in this isomer are closer to perfluoroadamantane values; meanwhile, CC(F)C angles are still abnormal (98.8°, 113.8°, and 115.8° for ∠**ce**, ∠**de**, and ∠**dc**, respectively), and more importantly, 10 double bonds (type **f**) are imposed into pentagons which are utterly energetically unfavorable. Hence, structure **II** is 478 kJ/mol (462 kJ/mol with zero-point vibrational energy correction) less stable than the "saturnene" isomer at the PBE/TZ2P level of theory (cf. semiempirical calculations were previously reported as 336 (AM1), 372 (PM3), or 544 kJ/mol (MNDO).[1]

Structure Elucidation from the Vibrational Spectra. The experimental IR spectrum of $C_{60}F_{20}$ and the calculated spectra for isomers **I** and **II** are presented in Figure 3. Comparison of the IR spectrum obtained in this work with the one published previously[1] shows in the latter a considerably larger number of lines in the C−F stretching region due to the contribution from the impurities ($C_{60}F_{20}O$, $C_{60}F_{14}$, and $C_{60}F_{12}$) which coelute with the $C_{60}F_{20}$ fraction in the Buckyprep column. It was due to the use of the two-stage HPLC separation that we were able to remove those impurities from the $C_{60}F_{20}$ sample and obtain a better IR spectrum (see for details the Experimental Section).

The dominating absorption in the whole frequency range is found at 1124 cm^{-1} in the characteristic region of C−F stretching vibrations. As follows from the spectra simulation, one very strong C−F band is indeed expected for both isomers. Despite the fact that the observed value is closer to the predicted wavenumber of such a vibration in isomer **I** than in isomer **II**, this spectral region does not provide sufficiently valuable information for structure elucidation. Vibrations of the carbon skeleton, especially in the 400−1000 cm^{-1} range, are much more characteristic for a specific isomer. One can clearly see that the calculated spectrum for structure **I** perfectly matches the experimental IR spectrum in the entire range—both in the relative band positions and in relative intensities, whereas the spectral pattern for isomer **II** is quite different (Figure 3). For example, each of the observed weak bands at 541, 559, 642, 731, 758, and 827 cm^{-1} as well as the medium absorptions at 949 and 982 cm^{-1} have their counterparts in the simulated spectrum of the "saturnene", and none of them can be found in the predicted spectrum of isomer **II**. Above 1200 cm^{-1}, a

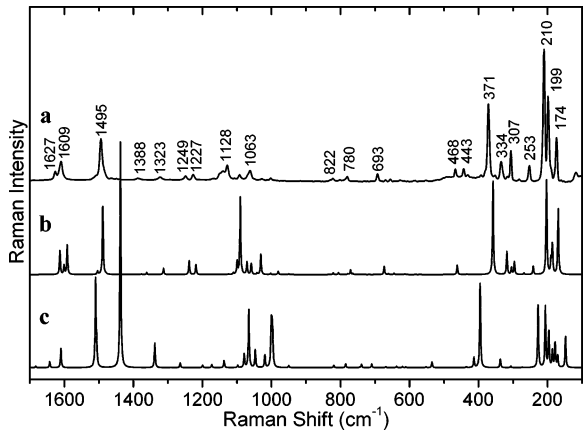

Figure 4. Raman spectra of $C_{60}F_{20}$: (a) experimental; (b) simulated for isomer **I** (saturnene); (c) simulated for isomer **II**.

number of relatively intense peaks are predicted for isomer **II**, but they are not present in the observed spectrum; instead, it contains only weak features at 1256, 1379, and 1622 cm^{-1}—in excellent agreement with the calculated spectrum of isomer **I**.

The Raman spectrum of $C_{60}F_{20}$ is measured in this work for the first time (Figure 4). Contrary to the IR absorption spectrum, C−F vibrations in the Raman spectrum possess only moderate intensity, while the strongest lines are observed in the 150−400 cm^{-1} range and at 1495 cm^{-1}. Apart from the somewhat underestimated frequencies in the 1000−1200 cm^{-1} region, the calculated Raman spectrum of "saturnene" (Figure 4b) perfectly reproduces the measured band positions and relative intensities. On the contrary, the simulated spectrum of isomer **II** (Figure 4c) does not match the experimental pattern in the 150−400 cm^{-1} range and contains a very strong line at 1437 cm^{-1} due to collective vibration of 10 double bonds in the equator of the molecule (type **f**, Figure 1b), a feature which is obviously absent in the experimental spectrum. Hence, comparison of the experimental and simulated IR and Raman spectra of $C_{60}F_{20}$ strongly favors the "saturnene" structure, in agreement with its higher thermodynamic stability. Thus, present results confirm earlier structural suggestions for a D_{5d} $C_{60}F_{20}$.[1]

Scaling and Assignment. In the framework of D_{5d} point symmetry, vibrational representation of "saturnene" $C_{60}F_{20}$ spans into

$$\Gamma_{vib}(C_{60}F_{20}) = 13A_{1g} + 10A_{2g} + 23E_{1g} + 24E_{2g} + 11A_{1u} + 12A_{2u} + 23E_{1u} + 24E_{2u}$$

symmetry types; of these, 35 modes of A_{2u} and E_{1u} symmetry are expected in the infrared spectra, and 60 modes of A_{1g}, E_{1g}, and E_{2g} symmetry are Raman-active. From these modes, 17 IR and 36 Raman modes were determined in the corresponding experimental spectra (Table 2).

While the relative positions and relative intensities of the bands in the experimental spectra are well reproduced in the simulated spectra, the predicted vibrational frequencies are shifted to lower values. Moreover, this underestimation is nonuniform within the whole frequency range, and maximum deviations (up to 40 cm^{-1}) are observed for ν(C−F) vibrations, while for lower and higher frequencies the difference is smaller: ca. 10−15 cm^{-1}. Similar shortcomings of the PBE/TZ2P approach were previously observed in our studies of $C_{60}F_{18}$[18] and $C_{60}F_{24}$,[19] and hence they are likely to possess systematic character.

TABLE 2: Computed and Experimental Frequencies (cm^{-1}) of "Saturnene" $C_{60}F_{20}$[a]

sym	DFT	scaled	obsd	sym	DFT	scaled	obsd	sym	DFT	scaled	obsd	sym	DFT	scaled	obsd
A_{1g}	169	173	174	A_{2g}	204	209		A_{1u}	182	187		A_{2u}	215	220	
	242	250	253		355	365			297	308			289	299	
	318	329	334		453	462			360	365			349	356	
	359	366	371		620	629			467	479			489	497	
	462	468	468		694	709			670	678			633	643	642
	661	669	669		820	835			683	694			717	730	731
	771	785	780		874	890			962	977			793	816	
	950	972			1084	1117			1011	1038			969	985	982
	1059	1080			1243	1259			1120	1154			1081	1114	
	1090	1129	1128		1431	1438			1273	1292			1243	1252	1256
	1238	1247	1249						1435	1443			1488	1496	
	1489	1497	1495	E_{2g}	172	175							1608	1620	
	1613	1626	1627		186	190	(199)	E_{1u}	168	172					
					203	207	210		199	204		E_{2u}	160	163	
E_{1g}	186	190	199		269	277	282		243	250			178	182	
	190	194	(199)		318	329	(334)		307	315			248	252	
	281	291			341	348	353		329	338			266	275	
	296	303	307		434	443	443		392	400			301	310	
	305	314	316		570	583			408	417	422		329	338	
	382	390	392		605	615			532	541	541		484	494	
	420	428	432		645	659	656		550	561	559		519	529	
	540	549			674	691	693		636	649	654		556	571	
	582	592			717	727			715	727			671	685	
	613	626	627		779	792			743	757	758		710	721	
	733	743			821	835	822		813	828	827		758	772	
	764	785			981	1005	1002		939	955	949		778	793	
	806	820	802		1031	1059	1063		969	994			807	821	
	883	897			1071	1091	1092		1059	1090	1090		942	961	
	1003	1030	1028		1100	1133	1141		1084	1122	1124		1016	1044	
	1042	1068			1141	1166			1121	1137	1147		1087	1116	
	1110	1137			1219	1228	1227		1186	1207			1105	1140	
	1125	1154			1313	1322	1323		1360	1370	1366		1175	1195	
	1225	1246			1377	1386	(1388)		1372	1381	1379		1217	1226	
	1361	1372			1504	1515	1505		1482	1492			1309	1319	
	1374	1383	1388		1592	1604	1609		1604	1618	1622		1380	1388	
	1480	1489											1501	1512	
	1601	1614	1614										1591	1603	

[a] The values in parentheses correspond to possible "double" assignment due to close vibrational frequencies of different modes.

TABLE 3: Internal Coordinates and Scaling Factors

internal coordinate	scaling factor	description of the internal coordinates
q(C═C)	1.0117	C═C double bonds (types **b**, **d**)
q(C^{sp2}−C^{sp2})	1.0067	ordinary C−C bonds in conjugated fragments of the molecule (types **a**, **c**)
q(C(F)−C^{sp2})	1.0144	ordinary C−C bonds between fluorine-bearing carbon atoms and C-sp^2 atoms in conjugated fragments of the molecule (type **e**)
q(C(F)−C(F))	1.0654	ordinary C−C bonds between fluorine-bearing carbon atoms (types **f**, **g**)
q(C−F)	1.0749	C−F bonds
γ(C−C^{sp2}−C)	1.0426	angles between two ordinary C−C bonds with C-sp^2 atom in the vertex (∠**aa**, ∠**cc**, ∠**ce**)
γ(C═C−C)	1.0072	angles between double and ordinary CC bonds (∠**ab**, ∠**bc**, ∠**cd**, ∠**de**)
γ(CC(F)C)	1.0419	angles between two ordinary C−C bonds with fluorine-bearing carbon atoms in the vertex (∠**ef**, ∠**eg**, ∠**fg**)
α(CCF)	1.0767	angles between C−F and adjacent C−C bonds

In this situation, a substantial improvement of the DFT results in vibrational calculations can be achieved by applying the Pulay scaling of quantum-chemical force fields.[20,21] Because of the universal character of the scaling factors in the groups of homologues or similar molecules, they can be used in vibrational simulations for unknown compounds within these groups. Hence, having obtained a reliable set of scaling factors for a known molecule (or a series of molecules), one can then apply the scaling procedure for similar molecules with yet unknown structures.

With this respect, $C_{60}F_{20}$ offers a unique opportunity for tuning the set of scaling factors for the whole family of fluorofullerenes. On the one hand, because of the high symmetry, this molecule possesses relatively simple and easy-to-assign vibrational spectra. On the other hand, observation of the sufficiently large number of the experimental frequencies in both Raman and IR spectra guarantees a stable inverse problem solution. We introduced nine scaling factors, one for each set of the chemically equivalent internal coordinates (see Table 3), and refined their values in the least-squares fitting of the calculated frequencies to the experimental values. The procedure resulted in the considerable improvements of the correspondence between the calculated and experimental frequencies, as can be seen in Tables 2 and 4. After scaling, the root-mean-square deviations in frequencies were reduced to 5 cm^{-1} (cf. 17 cm^{-1} for unscaled results), with the maximum discrepancy being only 18 cm^{-1} (cf. 40 cm^{-1} for the raw, unscaled data).

Assignment of the Vibrational Spectra. Because of the excellent agreement between the experimental and calculated IR and Raman spectra of $C_{60}F_{20}$, we were able to perform a complete assignment of the experimental spectral bands for this molecule (Table 4). The vibrational displacements of the most prominent modes are demonstrated in Figure 5. We have recently shown that interpretation of the vibrational modes of the $C_{60}X_n$ derivatives can be more favorable on the basis of the parent C_{60} vibrations (i.e., with the help of projection analysis[22]) than with the use of the conventional potential energy distribution (PED) analysis, which often yields nearly uniform distribution of the potential energy among various internal coordinates due to the complex interconnected character of the vibrations in the closed-cage molecules. Nonetheless, for some modes, such as bending CCX vibrations (where X is an addend), the PED interpretation is obviously more constructive. As a consequence, the vibrational assignment for $C_{60}F_{20}$ discussed below (and presented in Table 4) was obtained by combination of the projection and PED analyses. When expanding vibrations of the $C_{60}F_{20}$ carbon skeleton in terms of the C_{60} normal modes, the expansion coefficients, a_{ij}, were obtained as a result of scalar multiplication:

$$a_{ij} = (Q_i, Q_j)$$

where Q_i and Q_j are the mass-weighed Cartesian vibrational eigenvectors of C_{60} and $C_{60}F_{20}$ molecules, respectively. The squares of the expansion coefficients, a_{ij}^2, play the same role as percentage of a given internal coordinate in the PED analysis, and their sum (designated as d in Table 4) characterizes the fraction of carbon atom displacements in a given vibration of $C_{60}F_{20}$.

Three strong Raman lines at 174, 199, and 210 cm^{-1} correspond to the deformations of CCF angles mixed with the vibrations of the carbon skeleton. The contribution of CCF deformations in the potential energy of these modes constitutes about 30%; the cage deformations are correlated with the 5-fold degenerate $H_g(1)$ mode of C_{60} at 273 cm^{-1} (Figure 5b; see Table 5 for correlation of I_h and D_{5d} irreducible representations). Less intense Raman bands at 253, 307, and 334 cm^{-1} are purely CCF deformations, while a strong line at 371 cm^{-1} belongs to the skeleton vibration which originates from $A_g(1)$ C_{60} mode at 497 cm^{-1}. Note that the carbon atom displacements contribute less than 50% for most of the $C_{60}F_{20}$ vibrations below 400 cm^{-1}.

In the 400−800 cm^{-1} region, contributions of CCF deformations constitute 20−25% of the total potential energy, and vibrations of $C_{60}F_{20}$ molecule can be described as radial deformations of its carbon skeleton. These moderate intensity modes are observed at 443, 468, 656, 669, 693, 780, and 822 cm^{-1} in the Raman spectrum and at 422, 541, 559, 642, 731, 758, and 827 cm^{-1} in the IR spectrum. The odd modes have rather complex forms and in terms of C_{60} vibrations are described mostly by linear combinations of several modes with comparable contributions. On the contrary, parent C_{60} modes can be traced more confidently in the $C_{60}F_{20}$ Raman modes: e.g., $G_g(1)$ C_{60} vibration at 485 cm^{-1} contributes to 443 cm^{-1} E_{2g} $C_{60}F_{20}$ mode, and the 468 cm^{-1} A_{1g} $C_{60}F_{20}$ mode is mostly due to the component of $H_g(2)$ C_{60} vibration at 433 cm^{-1}, whereas dominating contribution to 693 cm^{-1} E_{2g} vibration of $C_{60}F_{20}$ belongs to $H_g(4)$ parent C_{60} mode at 772 cm^{-1}. Two medium IR absorptions at 949 and 982 cm^{-1} originate from $G_u(4)$ and $F_{2u}(3)$ tangential modes of C_{60} at 962 and 956 cm^{-1}, respectively, with the main contribution into potential energy arising from C−C elongations (Figure 5c).

C−F stretching modes partially mixed with ν(C−C) vibrations in the fluorinated fragment of $C_{60}F_{20}$ fall into the 1000−1200 cm^{-1} region, and they are observed as a very strong IR band at 1124 cm^{-1} (Figures 3 and 5d) and a group of the weak Raman lines at 1063, 1092, and 1128 cm^{-1} (Figure 4). Above 1200 cm^{-1}, the IR spectrum is very poor, with two weak bands at 1256 and 1379 cm^{-1} detected in the C−C stretching region and one absorption at 1622 cm^{-1} with the predominant C═C stretching character. In the framework of the projection analysis, these vibrations of $C_{60}F_{20}$ are related to $F_{1u}(3)$ (1182 cm^{-1}), $G_u(5)$ (1308 cm^{-1}), and $H_u(7)$ (1567 cm^{-1}) parent C_{60} modes. In the Raman spectrum, ν(C−C) vibrations are observed as weak

TABLE 4: Experimental vs Selected Calculated (Scaled) Vibrational Frequencies (ν, cm^{-1}) and Relative Intensities (int, %) of $C_{60}F_{20}$ with the Spectra Assignment

	calcd		obsd		assignment[a]	
sym	ν	int[b]	ν int	d,[c] %	C_{60} modes,[d] %	PED,[e] %
Raman modes						
A_{1g}	173	56.8	174 s	70	68 $H_g(1)$	32 γ(CC(F)C), 24 q(C−C), 18 γ(C−C^{sp2}−C)
E_{2g}	190	6.8		18		45 α(CCF), 23 γ(C═C−C), 16 γ(CC(F)C)
E_{1g}	190	26.0	199 s	26	19 $H_g(1)$	38 α(CCF), 22 γ(C═C−C), 21 γ(CC(F)C), 20 q(C−C)
E_{1g}	194	15.5		54	47 $H_g(1)$	23 α(CCF), 21 q(C−C), 17 γ(C−C^{sp2}−C), 16 γ(CC(F)C), 16 γ(C═C−C)
E_{2g}	207	100.0	210 vs	48	43 $H_g(1)$	29 γ(C═C−C), 22 γ(CC(F)C), 18 α(CCF), 17 q(C−C)
A_{1g}	250	7.4	253 m	9		73 α(CCF)
E_{2g}	277	1.62	282 vw	16		56 α(CCF), 19 q(C−C), 15 γ(CC(F)C)
E_{1g}	303	13.1	307 m	48	15 $H_g(1)$, 15 Rot-Tr	58 α(CCF), 23 γ(C═C−C)
E_{1g}	314	5.5	316 vw	19		70 α(CCF)
E_{2g}	329	4.9		5		86 α(CCF)
A_{1g}	329	12.9	334 m	9		79 α(CCF)
E_{2g}	348	1.1	353 vw	68	51 $H_g(2)$	44 γ(CC(F)C), 26 γ(C═C−C), 20 α(CCF)
A_{1g}	366	71.5	371 s	62	50 $A_g(1)$	68 q(C−C)
E_{1g}	390	0.0	392 vw	48	31 $H_g(2)$	43 γ(CC(F)C), 21 α(CCF), 17 γ(C═C−C)
E_{1g}	428	0.0	432 vw	65	44 $G_g(1)$	26 γ(C═C−C), 22 γ(CC(F)C), 19 α(CCF), 15 q(C−C)
E_{2g}	443	1.1	443 w	81	60 $G_g(1)$	29 α(CCF), 24 γ(C═C−C), 21 γ(CC(F)C)
A_{1g}	468	10.5	468 w	89	77 $H_g(2)$	43 γ(C═C−C), 17 α(CCF)
E_{1g}	626	2.2	627 vw	83	41 $H_g(3)$, 24 $F_{1g}(1)$	39 γ(C═C−C), 22 α(CCF), 19 γ(CC(F)C)
E_{2g}	659	1.2	656 vw	73	47 $G_g(2)$	27 γ(C═C−C), 21 α(CCF), 16 q(C−F)
A_{1g}	669	0.7	669 vw	100	78 $H_g(3)$	46 γ(C═C−C), 26 γ(C−C^{sp2}−C)
E_{2g}	691	4.6	693 w	91	50 $H_g(4)$, 18 $G_g(2)$	34 q(C−C), 27 α(CCF), 19 γ(C−C^{sp2}−C)
A_{1g}	785	1.5	780 w	90	49 $H_g(4)$, 18 $A_g(1)$, 16 $H_g(3)$	35 q(C−C), 18 α(CCF)
E_{1g}	820	0.9	802 vw	93	72 $H_g(4)$	29 α(CCF), 29 q(C−C), 15 γ(C═C−C)
E_{2g}	835	1.6	822 vw	98	78 $F_{2g}(3)$	43 γ(C═C−C), 19 α(CCF)
E_{2g}	1005	3.0	1002 vw	93	mixed character	36 q(C−C), 21 γ(CC(F)C), 15 q(C−F)
E_{1g}	1030	3.1	1028 vw	82	mixed character	44 q(C−F), 21 γ(CC(F)C), 19 q(C−C)
E_{2g}	1059	21.2	1063 w	82	mixed character	53 q(C−F), 17 q(C−C)
E_{2g}	1091	7.8	1092 w	87	mixed character	36 q(C−C), 34 q(C−F)
A_{1g}	1129	36.2	1128 m	72	mixed character	80 q(C−F), 15 q(C−C)
E_{2g}	1133	11.0	1141 sh	92	mixed character	38 q(C−C), 31 q(C−F)
E_{2g}	1228	2.3	1227 w	100	49 $G_g(4)$, 22 $H_g(6)$	73 q(C−C), 16 γ(C═C−C)
A_{1g}	1247	3.2	1249 w	100	54 $H_g(6)$, 40 $H_g(5)$	70 q(C−C)
E_{2g}	1322	13.0	1323 w	100	49 $G_g(5)$, 18 $H_g(6)$	55 q(C−C), 26 γ(C═C−C)
E_{1g}	1383	2.0	1388 w	100	59 $G_g(5)$, 29 $H_g(6)$	48 q(C−C), 30 γ(C═C−C)
E_{2g}	1386	1.9		100	52 $F_{2g}(4)$, 22 $G_g(5)$, 20 $H_g(6)$	46 q(C−C), 33 γ(C═C−C)
A_{1g}	1497	84.6	1495 s	100	61 $A_g(2)$, 35 $H_g(7)$	63 q(C═C), 31 q(C−C)
E_{2g}	1515	0.8	1505 sh	100	58 $G_g(6)$, 33 $H_g(7)$	51 q(C═C), 25 q(C−C)
E_{2g}	1604	23.5	1609 m	100	85 $H_g(8)$	45 q(C═C), 20 q(C−C), 18 γ(C═C−C), 16 γ(C−C^{sp2}−C)
E_{1g}	1614	6.1	1614 sh	100	53 $G_g(6)$, 41 $H_g(8)$	48 q(C═C), 20 q(C−C), 18 γ(C−C^{sp2}−C)
A_{1g}	1626	10.8	1627 w	100	84 $H_g(8)$	56 q(C═C), 18 q(C−C)
IR modes						
E_{1u}	417	0.5	422 w	61	25 $F_{1u}(1)$, 20 $F_{1u}(2)$	28 q(C−C), 27 γ(CC(F)C), 25 γ(C═C−C)
E_{1u}	541	1.0	541 vw	76	26 $F_{1u}(1)$, 16 $H_u(2)$	35 γ(C═C−C), 25 α(CCF), 19 q(C−C)
E_{1u}	561	1.1	559 w	92	46 $H_u(2)$, 23 $H_u(1)$	29 γ(C−C^{sp2}−C), 26 α(CCF), 25 γ(C═C−C)
A_{2u}	643	2.3	642 w	90	53 $F_{1u}(2)$, 30 $F_{2u}(2)$	26 q(C−C), 21 γ(C═C−C), 16 γ(C−C^{sp2}−C), 15 α(CCF)
E_{1u}	649	0.4	654 vw	74	30 $F_{1u}(1)$, 18 $H_u(4)$	39 γ(C═C−C), 20 α(CCF), 15 q(C−F)
A_{2u}	730	3.2	731 m	96	51 $F_{2u}(2)$, 32 $F_{1u}(2)$	26 γ(C═C−C), 25 α(CCF), 20 q(C−C), 17 γ(C−C^{sp2}−C)
E_{1u}	757	0.5	758 w	97	44 $G_u(2)$, 35 $H_u(4)$	34 γ(C−C^{sp2}−C), 21 α(CCF), 19 γ(C═C−C)
E_{1u}	828	0.4	827 vw	96	30 $G_u(3)$, 27 $G_u(2)$, 26 $H_u(4)$	41 γ(C═C−C), 31 α(CCF)
E_{1u}	955	9.4	949 m	94	60 $G_u(4)$	35 q(C−C), 20 γ(CC(F)C)
A_{2u}	985	8.8	982 m	88	72 $F_{2u}(3)$	47 q(C−C), 26 q(C−F)
E_{1u}	1090	6.2	1090 sh	83	30 $G_u(3)$, 19 $F_{1u}(3)$	56 q(C−F)
E_{1u}	1122	100.0	1124 vs	76	mixed character	71 q(C−F), 17 q(C−C)
E_{1u}	1137	12.9	1147 sh	99	27 $H_u(5)$, 24 $G_u(4)$, 21 $F_{1u}(4)$	57 q(C−C)
A_{2u}	1252	0.5	1256 vw	100	71 $F_{1u}(3)$, 22 $F_{2u}(4)$	71 q(C−C)
E_{1u}	1370	0.0	1366 vw	100	69 $H_u(6)$	47 q(C−C), 33 γ(C═C−C), 16 γ(C−C^{sp2}−C)
E_{1u}	1381	1.1	1379 vw	100	65 $G_u(5)$	49 q(C−C), 30 γ(C═C−C)
E_{1u}	1618	0.8	1622 w	100	82 $H_u(7)$	48 q(C═C), 20 q(C−C), 19 γ(C−C^{sp2}−C)

[a] Contributions less than 15% are omitted. [b] Relative intensities are % for calculated bands and are very strong (vs), strong (s), medium (m), weak (w), very weak (vw), or shoulder (sh) for observed bands. [c] d = total contribution of carbon skeleton displacements into the vibration of $C_{60}F_{20}$. [d] "Mixed character" denotes that vibrations of carbon skeleton were described as a combination of several C_{60} modes without any dominating one. [e] Contributions of all ordinary CC bonds are summed up and designated as q(C−C).

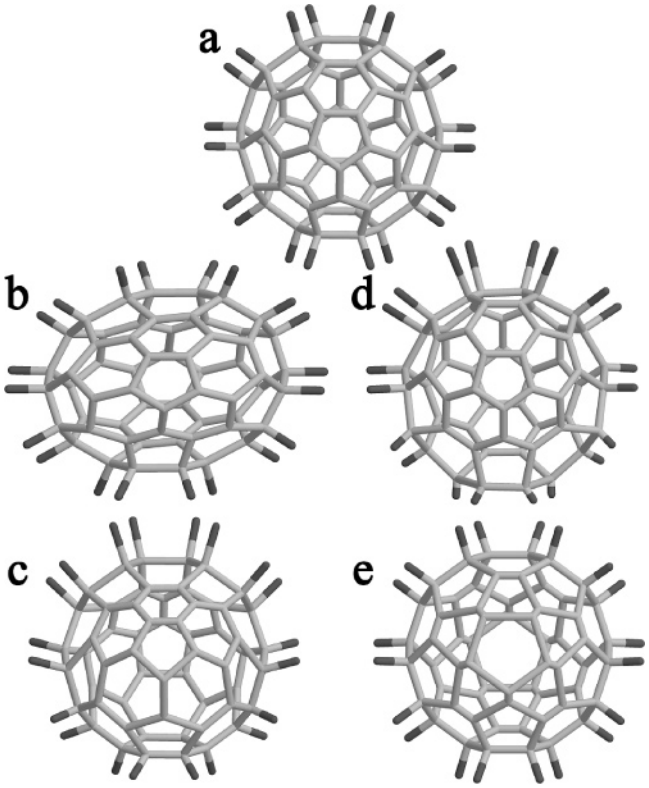

Figure 5. Equilibrium configuration of $C_{60}F_{20}$ molecule (a) and displacements for the indicated normal modes of vibration: E_{2g} at 210 cm^{-1} (b), E_{1u} at 949 cm^{-1} (c), E_{1u} at 1124 cm^{-1} (d), and A_{1g} at 1495 cm^{-1} (e).

TABLE 5: Correlation Table for I_h and D_{5d} Point Symmetry Groups[a]

I_h (C_{60})	D_{5d} ($C_{60}F_{20}$)
A_g(Ram)	A_{1g}(Ram)
F_{1g}	$A_{2g} + E_{1g}$(Ram)
F_{2g}	$A_{2g} + E_{2g}$(Ram)
G_g	E_{1g}(Ram) + E_{2g}(Ram)
H_g(Ram)	A_{1g}(Ram) + E_{1g}(Ram) + E_{2g}(Ram)
A_u	A_{1u}
F_{1u}(IR)	A_{2u}(IR) + E_{1u}(IR)
F_{2u}	A_{2u}(IR) + E_{2u}
G_u	E_{1u}(IR) + E_{2u}
H_u	$A_{1u} + E_{1u}$(IR) + E_{2u}

[a] Raman or infrared activity of the vibrations is designated by "Ram" or "IR" in parentheses.

lines at 1227, 1249, 1323, and 1388 cm^{-1}, while the intensity of C═C stretching is much higher: a strong line at 1495 cm^{-1} belongs to the analogue of $A_g(2)$ C_{60} vibration at 1468 cm^{-1} (Figure 5e), and peaks at 1609, 1614 (sh), and 1627 cm^{-1} are related to $H_g(8)$ C_{60} mode at 1575 cm^{-1}. Noteworthy, ν(C−C) and ν(C═C) vibrations in the conjugated part of the fluorofullerene molecule are hardened considerably as compared to the corresponding modes of the pristine fullerene.

Conclusions

A comprehensive vibrational spectroscopic analysis has been performed for the first time for the fluoro[60]fullerene molecule, $C_{60}F_{20}$. An excellent correspondence between the calculated and experimental IR and Raman spectra, along with the scaling of the DFT force field, enabled us to perform a complete vibrational assignment for $C_{60}F_{20}$. These results provide a redundant proof for the original conjecture of the $C_{60}F_{20}$ structure with the equatorial belt of 20 fluorine atoms on C_{60} cage. The alternative structure is ruled out on the basis of the vibrational spectroscopic data and DFT calculated energies.

The scaling factors, obtained in this work for one fluorofullerene molecule—$C_{60}F_{20}$—possess universal character; i.e., they are transferable within the whole class of the fluorinated fullerenes. Therefore, it now becomes possible to perform (i) complete interpretation of the vibrational spectral data for the fluorofullerenes with the known structures, (ii) comparative vibrational analysis for the compounds with uncertain structural assignments, often based only on NMR data, and (iii) predictions of the most probable structures for new fluorofullerenes using available vibrational and NMR spectroscopic data.

The reliability of this approach has been proven by our preliminary calculations performed for $C_{60}F_{18}$ and $C_{60}F_{48}$ (both compounds with well-established structures), which demonstrated excellent agreement with the experimental vibrational spectra.[18,23] Earlier, a good correlation between the computed and observed vibrational data was achieved for other halofullerene with known structure T_h $C_{60}Br_{24}$.[22] Furthermore, a similar approach was applied in order to predict the most probable structure of the new bromo[70]fullerene, for which the IR spectrum was measured.[24] The agreement between the simulated IR spectrum of one of the structures of $C_{70}Br_{10}$ molecule with the experimental IR data served as a basis for the tentative structural conjecture, and later it was confirmed by X-ray single-crystal structural data.[25]

In summary, these examples, together with the new results on $C_{60}F_{20}$, clearly demonstrate high potential of the approach described in the present work: application of the experimental vibrational spectroscopy (both Raman and IR) in combination with the theoretical analysis may offer an effective solution for complex problems of structure elucidation, when the X-ray single crystal structural data are not available or NMR data are either not available or not sufficient for unambiguous structure assignment. Both spectroscopic techniques do not require considerable amounts of the pure material (or good solubility as for NMR) for recording good-quality spectra. This may allow one to broaden considerably the number and types of fullerene derivatives for structural elucidation, which otherwise could not be characterized—either because of the low solubility, instability in solution, or insufficient quantities of the purified samples. Other halofullerenes, such as bromides and chlorides, can be studied, if a special care is taken in recording Raman spectra of these compounds, which were reported to be subject to dehalogenation under laser irradiation.

Finally, in the course of this work, a significant progress has been made in the synthesis of fluorofullerenes with low fluorine content. We succeeded in fine-tuning of the fluorination degree of C_{60} toward molecules with lower F content either by diluting strong fluoroagent MnF_3 with KF or by using ternary fluoride, Li_4CeF_8, instead of more reactive binary fluoride, CeF_4. This result, in combination with the improved two-stage HPLC purification schemes described in this work, makes a large number of F-containing fullerene derivatives available for future detailed spectroscopic studies.

Acknowledgment. This work was supported by the Volkswagen Foundation (I-77/855) and the Russian Foundation for Basic Research (03-03-32855 and 03-03-32179). O.V.B. is grateful to Humboldt Foundation for generous support through the F. Bessel award. We thank Dr. S. Lebedkin for his invaluable support of the work of I.E.K.

References and Notes

(1) Boltalina, O. V.; Markov, V. Y.; Troshin, P. A.; Darwish, A. D.; Street, J. M.; Taylor, R. *Angew. Chem., Int. Ed.* **2001**, *40*, 787.

(2) Sandall, J. P. B.; Fowler., P. W. *Org. Biomol. Chem.* **2003**, *1*, 1061.
(3) Boltalina, O. V.; Darwish, A. D.; Street, J. M.; Taylor, R.; Wei, X.-W. *J. Chem. Soc., Perkin Trans. 2* **2002**, 251.
(4) Gakh, A. A.; Tuinman, A. A. *Tetrahedron Lett.* **2001**, *42*, 7137.
(5) Boltalina, O. V.; Goryunkov, A. A.; Markov, V. Y.; Ioffe, I. N.; Sidorov, L. N. *Int. J. Mass Spectrom.* **2003**, *228*, 807.
(6) A.Delaigue, J.-C. C. *Rev. Chim. Miner.* **1972**, *9*, 789.
(7) Lukonin, A. Y.; Markov, V. Y.; Boltalina, O. V. *Vestnik Moscov. Univ. Ser. 2: Khim.* **2001**, *42*, 3.
(8) Laikov, D. N. *Chem. Phys. Lett.* **1997**, *281*, 151.
(9) Perdew, J. P.; Burke, K.; Ernzerhof, M. *Phys. Rev. Lett.* **1996**, *77*, 3865.
(10) Granovsky, A. A. PC GAMESS URL: http://classic.chem.msu.su/gran/gamess/index.html.
(11) Schmidt, M. W.; Baldridge, K. K.; Boatz, J. A.; Elbert, S. T.; Gordon, M. S.; Jensen, J. H.; Koseki, S.; Matsunaga, N.; Nguyen, K. A.; Su, S. J.; Windus, T. L.; Dupuis, M.; Montgomery, J. A. *J. Comput. Chem.* **1993**, *14*, 1347.
(12) Yagola, A. G.; Kochikov, I. V.; Kuramshina, G. M.; Pentin, Y. A. *Inverse Problems of Vibrational Spectroscopy*; VSP: Zeist, 1999.
(13) Lukonin, A. Y. Synthesis of fluorofullerenes in reactions with inorganic fluorides and some physical chemical properties. Ph.D. Dissertation, Moscow State University, 2002.
(14) Hargittai, I.; Brunvoll, J.; Sonoda, T.; Abe, T.; Baba, H. *J. Mol. Struct. (THEOCHEM)* **1998**, *445*, 55.
(15) Neretin, I. S.; Lyssenko, K. A.; Antipin, M. Y.; Slovokhotov, Y. L.; Boltalina, O. V.; Troshin, P. A.; Lukonin, A. Y.; Sidorov, L. N.; Taylor, R. *Angew. Chem., Int. Ed.* **2000**, *39*, 3273.
(16) Hitchcock, P. B.; Taylor, R. *Chem. Commun.* **2002**, 2078.
(17) Troyanov, S. I.; Troshin, P. A.; Boltalina, O. V.; Ioffe, I. N.; Sidorov, L. N.; Kemnitz, E. *Angew. Chem., Int. Ed.* **2001**, *40*, 2285.
(18) Rau, J. V.; Nunziante Cesaroa, S.; Boltalina, O. V.; Agafonov, V.; Popov, A. A.; Sidorov, L. N. *Vib. Spectrosc.* **2004**, *34*, 137.
(19) Denisenko, N. I.; Troyanov, S. I.; Popov, A. A.; Kuvychko, I. V.; Zemva, B.; Kemnitz, E.; Strauss, S. H.; Boltalina, O. V. *J. Am. Chem. Soc.* **2004**, *126*, 1618.
(20) Pulay, P.; Fogarasi, G.; Pongor, G.; Boggs, J. E.; Vargha, A. *J. Am. Chem. Soc.* **1983**, *105*, 7037.
(21) Baker, J.; Jarzecki, A. A.; Pulay, P. *J. Phys. Chem. A* **1998**, *102*, 1412.
(22) Popov, A. A.; Senyavin, V. M.; Granovskiy, A. A. *Chem. Phys. Lett.* **2004**, *383*, 149.
(23) Popov, A. A.; et al., unpublished data.
(24) Denisenko, N. I.; Popov, A. A.; Kouvitchko, I. V.; Boltalina, O. V.; Chelovskaya, N. V. *Proc. Electrochem. Soc.* **2002**, *2002-12*, 577.
(25) Troyanov, S. I.; Denisenko, N. I.; Popov, A. A.; Boltalina, O. V.; Kemnitz, E. *Angew. Chem., Int. Ed.* **2003**, *42*, 2395.